Journal of Sound and Vibration (1996) **192**(3), 645–668

DYNAMICS OF AN ARTICULATED CYLINDER IN ANNULAR FLOW VIA NON-LINEAR AND PARTIALLY LINEARIZED VERSIONS OF AN ANALYTICAL MODEL

R. M. Botez and M. P. Païdoussis

Department of Mechanical Engineering, McGill University, Sherbrooke Street-West, Montréal, Québec, Canada, H3A 2K6

(*Received* 9 *September* 1994, *and in final form* 16 *August* 1995)

This paper deals with the non-linear dynamics of an articulated system of two rigid cylinders interconnected by rotational springs, within a pipe conveying fluid, with fluid flowing downward in the relatively narrow annular space. The impacting of the articulated cylinder system on the external pipe is modelled by a cubic spring. The behaviour of the articulated cylinder system is studied for flow velocities higher than the critical value at which a flutter or a divergence instability occurs. Two models are constructed for this system, depending on the form of equations of motion considered: in the first model, the dynamics of the system when no impact occurs with the outer pipe is described by a set of non-linear equations in which the non-linearities are taken into account approximately to order three via Taylor expansions of the trigonometric functions of state variables; in the second case, these equations are linearized. For both models, the dynamical behaviour of the system is illustrated by phase plane portraits, bifurcation diagrams, power spectra and Poincaré sections. The results obtained via these two models are compared qualitatively and quantitatively.

1. INTRODUCTION

Interest in the behaviour of *articulated* cylindrical systems in external axial flow is more recent than for continuous (distributed parameter) systems in axial flow. Work was done (1) in conjunction with the dynamics of fuel "strings" or "stringers" of certain types of nuclear reactor [1], and (2) underwater systems towed by a submarine [2, 3]. The fuel strings consist of fuel bundles held together by a central support tube; the string is mounted vertically within a pressure tube, and it is supported at the bottom end and free on top, with the flow upwards. The theoretical study by Païdoussis [1] is of special interest here, since the physical system in that paper is quite similar to that considered in the present study and, hence, so are the equations of motion—although in the case of the fuel string they are considerably more complex.

The second example, is the concept of a "Sea Chain System", which was proposed in the early 1970s [2]. The "Sea Chain" is a submarine system consisting of a power module pulling a series of quasi-cylindrical freight modules, all connected by flexible couplings. This system is suited for operation in the Arctic as a transportation system for oil, gas and bulk cargo, its advantages being that: (1) it avoids the difficulties associated with surface transport in ice-infested waters; (2) it is highly manoeuvrable; (3) it is adaptable to transporting different cargos, simply by changing modules. This system is similar to the

0022–460X/96/180645 + 24 $18.00/0

Dracone, a semi-submerged, highly flexible, sausage-like container towed behind a small craft [4, 5], which is used for the transportation of oil and other lighter than sea-water cargo, including fresh water, to arid lands (e.g., some of the Aegean islands from the Greek mainland).

Also of interest to the present study is the work on "pendular oscillations" of articulated systems modelling nuclear reactor reactivity monitoring or control systems [6, 7], where the cylindrical elements are hung in the form of simple or compound pendula within a tube and are cooled by annular flow.

This paper describes the non-linear dynamical behaviour of a system of the type shown in Figure 1(a): an articulated system of cylinders interconnected by rotational springs, within a pipe containing flowing fluid. Two models were constructed for this system, one non-linear and the other linearized (apart from impact-related forces), and the two sets of results obtained are compared.

With the recent interest in chaotic motions of non-linear systems [8, 9], it seems appropriate to look into the possible existence of chaos in the system considered, once the articulated cylinder impacts on the external pipe. The chaotic motions of the system described by the linearized model have been studied before by Païdoussis and Botez [10], for different parameters. Moreover, it was shown [11] that, by varying only two parameters, this system may become chaotic via the (1) period-doubling, (2) quasiperiodic, and (3) intermittency routes.

2. EQUATIONS OF MOTION

2.1. DESCRIPTION OF THE SYSTEM AND ASSUMPTIONS

The articulated system here under consideration consists of a number, N, of rigid cylinders (in the cases considered here, $N = 2$) interconnected by rotational springs, with the lowest cylinder being terminated by a more or less streamlined, ogival end. The system is located in the centre of a pipe (Figure 1(a)), and it is pinned at the upstream end and free at the downstream one. Fluid flows downward in the narrow annular space between the pipe and the articulated system.

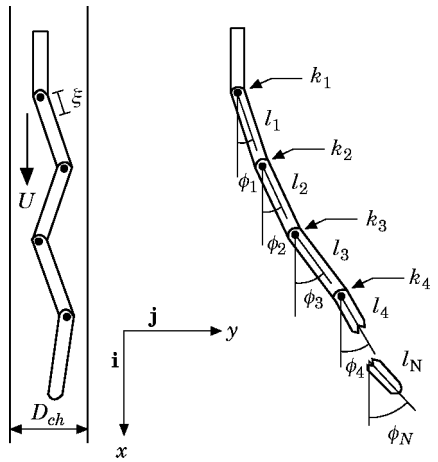

(a) (b)

Figure 1. (a) Diagram of the articulated cylindrical system in a confining channel, subjected to a mean annular flow of velocity, U; (b) definition diagram for the generalized coordinates ϕ_j, $j = 1, \ldots, N$, showing the cylinder lengths l_j and interconnecting springs of stiffnesses k_j.

In the interests of simplicity of analysis, the following assumptions are made: (a) the fluid is taken to be incompressible; (b) the articulated cylinder system is considered to be slender, as the diameter of the articulated cylinders is small compared to their length; (c) motions of the articulated system are considered to be planar; (d) as the annular space between the articulated cylinder system and the outer pipe is small and small angles of deformation are involved, it is assumed that there is no local separation of the flow as the system oscillates; (e) the impacting between the articulated cylinder system and the outer pipe is modelled realistically by a trilinear spring, but, for analytical convenience, also by a cubic spring. In the present paper, only the cubic spring model is utilized.

Although the fluid forces could in principle be determined by an appropriate solution of the Navier-Stokes equations, this will not be attempted here and instead the fluid forces will be determined essentially by superposition: inviscid and viscous forces will be formulated separately. This has been shown to be quite acceptable [12, 13] for the continuously flexible counterpart of the present problem, as well as for more complex systems [14]. Hence, the forces associated with the structure itself, i.e., the restoring, inertial and gravity forces acting on the structure, are taken into account in the kinetic and potential energies of the system. The hydrodynamic forces are incorporated partly in the kinetic energy and partly as generalized forces.

The equations of motion will be obtained by application of the Lagrange equations, for a system with an arbitrary number of articulated cylinders, N, although the calculations to be presented will be confined to $N = 2$. The lengths of the cylinders in the system are l_j, the interconnecting rotational spring stiffnesses are k_j, and the generalized coordinates chosen are the angles of deformation ϕ_j, where $j = 1, \ldots, N$, as shown in Figure 1(b).

Two models are constructed for this system: the first one including non-linear terms, and the second model with mainly linearized terms.

2.2. KINETIC AND POTENTIAL ENERGIES OF THE SYSTEM

2.2.1. Kinetic and potential energies of the articulated structure, T_s and V_s

In this section, the kinetic and potential energies of the articulated system itself, are determined in terms of the generalized coordinates.

The system of coordinates $(\mathbf{x}, \mathbf{y})$ with its corresponding system of unit vectors $(\mathbf{i}, \mathbf{j})$ have already been defined in Figure 1; the local coordinate ξ along the length of each cylinder segment, $0 \leqslant \xi \leqslant l_j$, is also defined in Figure 1. In order to calculate the velocity vector at point ξ of the jth cylinder, $\mathbf{v}_j(\xi)$, the displacements at that point in the x- and y-directions, $x_j(\xi)$ and $y_j(\xi)$, are calculated, as shown in Figure 1. The displacement vectors $\mathbf{x}_j(\xi)$ and $\mathbf{y}_j(\xi)$ at point ξ of the jth cylinder are

$$\mathbf{x}_j(\xi) = x_j(\xi)\mathbf{i} = -\left(\sum_{q=1}^{j-1} l_q \cos\phi_q + \xi \cos\phi_j\right)\mathbf{i},$$

$$\mathbf{y}_j(\xi) = y_j(\xi)\mathbf{j} = \left(\sum_{q=1}^{j-1} l_q \sin\phi_q + \xi \sin\phi_j\right)\mathbf{j}. \tag{1, 2}$$

Thus, $\mathbf{v}_j(\xi)$ is given by

$$\mathbf{v}_j(\xi) = \frac{\mathrm{d}}{\mathrm{d}t}\left[-\left(\sum_{q=1}^{j-1} l_q \cos\phi_q + \xi \cos\phi_j\right)\mathbf{i} + \left(\sum_{q=1}^{j-1} l_q \sin\phi_q + \xi \sin\phi_j\right)\mathbf{j}\right], \tag{3}$$

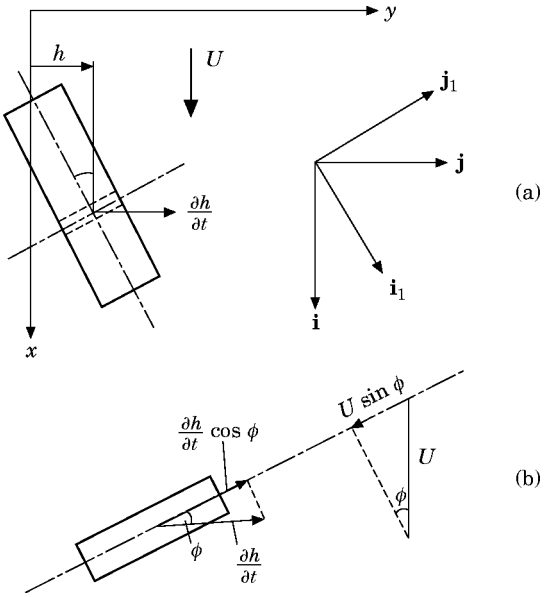

Figure 2. (a) Calculation of angle $\phi = \arctan \partial h/\partial x$ due to cylinder displacement $h(x, t)$ in the y direction; (b) calculation of the relative fluid-body velocity in the $\mathbf{j}_1$ direction.

which, after differentiation, may be written as

$$\mathbf{v}_j(\xi) = \left[\left(\sum_{q=1}^{j-1} l_q \sin\phi_q\dot{\phi}_q + \xi \sin\phi_j\dot{\phi}_j\right)\mathbf{i} + \left(\sum_{q=1}^{j-1} l_q \cos\phi_q\dot{\phi}_q + \xi \cos\phi_j\dot{\phi}_j\right)\mathbf{j}\right]. \tag{4}$$

Hence, the kinetic energy of the jth cylinder is

$$T_{sj} = \tfrac{1}{2}\int_0^{l_j} m_j\left[\left(\sum_{q=1}^{j-1} l_q \sin\phi_q\dot{\phi}_q + \xi \sin\phi_j\dot{\phi}_j\right)^2 + \left(\sum_{q=1}^{j-1} l_q \cos\phi_q\dot{\phi}_q + \xi \cos\phi_j\dot{\phi}_j\right)^2\right]\mathrm{d}\xi, \tag{5}$$

where m_j is the mass per unit length of the jth cylinder. The total kinetic energy of the structure, T_s, neglecting the small ogival part of the last cylinder, is

$$T_s = \tfrac{1}{2}\sum_{j=1}^{N}\int_0^{l_j} m_j\left[\left(\sum_{q=1}^{j-1} l_q \sin\phi_q\dot{\phi}_q + \xi \sin\phi_j\dot{\phi}_j\right)^2 + \left(\sum_{q=1}^{j-1} l_q \cos\phi_q\dot{\phi}_q + \xi \cos\phi_j\dot{\phi}_j\right)^2\right]\mathrm{d}\xi. \tag{6}$$

The potential energy is composed of a gravity component and a component due to strain of the intercylinder connecting springs. It may be written in the following form:

$$V_s = \sum_{j=1}^{N}\int_0^{l_j} m_j g\left[\sum_{q=1}^{j-1} l_q(1-\cos\phi_q) + \xi(1-\cos\phi_j)\right]\mathrm{d}\xi + \tfrac{1}{2}\sum_{j=1}^{N} k_j(\phi_j - \phi_{j-1})^2. \tag{7}$$

2.2.2. Kinetic energy of the fluid, T_f

In order to calculate the normal flow velocity at a point ξ of the jth cylinder, Figures 1 and 2 are reconsidered with the systems of unit vectors $(\mathbf{i}, \mathbf{j})$ and $(\mathbf{i}_1, \mathbf{j}_1)$, where $\mathbf{i}_1$ has the same direction as the long axis of the structure, and the $\mathbf{j}_1$-direction is normal to it.

The flow velocity of the jth cylinder is due to motion of the structure and to the flow in the confining pipe, and its components in the $\mathbf{i}_1$- and $\mathbf{j}_1$-directions will be

calculated next. The relative fluid-body velocity component in a direction normal to the element (i.e., in the $\mathbf{j}_1$-direction) at a point ξ of the jth cylinder, is defined as $v_{fj1}(\xi)$ and is given by

$$v_{fj1}(\xi) = -\frac{\mathrm{d}x_j(\xi)}{\mathrm{d}t}\sin\phi_j + \frac{\mathrm{d}y_j(\xi)}{\mathrm{d}t}\cos\phi_j + U\sin\phi_j, \tag{8}$$

where the displacements of the jth cylinder in the system, $x_j(\xi)$ and $y_j(\xi)$, have been defined in equations (1) and (2). The derivatives $\mathrm{d}x_j(\xi)/\mathrm{d}t$ and $\mathrm{d}y_j(\xi)/\mathrm{d}t$ have been calculated to obtain equation (4); by substituting them into equation (8), one obtains

$$v_{fj1}(\xi) = \sum_{q=1}^{j-1} l_q \cos(\phi_q - \phi_j)\dot{\phi}_q + \xi\dot{\phi}_j + U\sin\phi_j. \tag{9}$$

The fluid velocity component in the same direction as the element, i.e., in the $\mathbf{i}_1$-direction, is

$$v_{fi1}(\xi) = U\cos\phi_j. \tag{10}$$

Hence, the total velocity of the fluid at point ξ of the jth cylinder may be written as

$$\mathbf{v}_{fj}(\xi) = U\cos\phi_j\mathbf{i}_1 + \left[\sum_{q=1}^{j-1} l_q \cos(\phi_q - \phi_j)\dot{\phi}_q + \xi\dot{\phi}_j + U\sin\phi_j\right]\mathbf{j}_1, \tag{11}$$

and the kinetic energy of the fluid associated with the jth cylinder, T_{fj}, is

$$T_{fj} = \tfrac{1}{2}\int_0^{l_j} (U\cos\phi_j)^2 M_{i1}\,\mathrm{d}\xi + \tfrac{1}{2}\int_0^{l_j}\left[\sum_{q=1}^{j-1} l_q \cos(\phi_q - \phi_j)\dot{\phi}_q + \xi\dot{\phi}_j + U\sin\phi_j\right]^2 M_{j1}\,\mathrm{d}\xi, \tag{12}$$

where M_{i1} and M_{j1} are the corresponding virtual or "added" masses of the fluid in the $\mathbf{i}_1$- and $\mathbf{j}_1$-directions. As M_{i1} is much smaller than M_{j1}, usually of $O(\epsilon^2)$, then even if v_f in the i_1-direction is greater than v_f in the j_1-direction, i.e., $v_{fi1} > v_{fj1}$, since they are usually of the same order, $\frac{1}{2}M_{i1}v_{fi1}^2$ still remains much smaller than $\frac{1}{2}M_{j1}v_{fj1}^2$, possibly of order $O(\epsilon^2)$ or smaller. Clearly, for very slender cylinders it can be of much smaller order [15]. Hence, although the first term in equation (12) could have been retained, for convenience it will be neglected. M_{j1} is equal to $\chi\rho A$ for confined flow, where ρ is the fluid density, A the cylinder cross-sectional area, and

$$\chi = [(1+h)^2 + 1]/[(1+h)^2 - 1], \tag{13}$$

in which $h = D_h/D$; D is the cylinder diameter, and $D_h = D_{ch} - D$ is the hydraulic diameter, D_{ch} being the internal diameter of the external pipe. Consequently, the total fluid kinetic energy becomes

$$T_f = \tfrac{1}{2}\chi\rho A\int_0^{l_j}\left[\sum_{q=1}^{j-1} l_q \cos(\phi_q - \phi_j)\dot{\phi}_q + \xi\dot{\phi}_j + U\sin\phi_j\right]^2 \mathrm{d}\xi. \tag{14}$$

The inviscid forces acting on the cylinders of the articulated system will be obtained via this expression for the kinetic energy, once it is substituted into the Lagrange equations. Other fluid forces are formulated in the next section.

2.3. OTHER FLUID FORCES

The remaining fluid forces, other than those already taken into account in the kinetic energy, will be determined in several parts in the following subsections: a nonconservative inviscid force acting at the free end, hydrostatic forces and viscous forces.

2.3.1. Non-conservative inviscid force, F_{nc}

If both ends of the articulated system were supported, expression (14) would represent the whole of the inviscid component of the fluid-dynamic forces. The cantilevered system, however, is generally non-conservative, hence there will generally be work done at the free end of the system by a non-conservative inviscid force, F_{nc} [12, 16]. This force is associated with the non-cylindrical, ogival end of the last cylinder, which may be approximated by a paraboloid of the form $y^2(x) = 4a(w - x)$. In the present system, a is the focal distance of the downstream end, w is its total length, and $y(x)$ is the local radius of the paraboloid. For each shape, there is a form factor, f, such that for an ideally streamlined end, $f \to 1$, and for a blunt end, $f \to 0$; for different values for a and w, the corresponding value of f may be estimated empirically, $0 \leqslant f \leqslant 1$, as shown in Appendix A.

F_{nc}, acting at the end of a flexible cylinder, is found to be [16, 17]

$$F_{nc} = \rho(1 - f)\chi \int_0^w \left[\frac{\partial}{\partial t} + U\frac{\partial}{\partial x}\right] V_l 4\pi a(w - \xi)\,\mathrm{d}\xi. \tag{15}$$

Now, for the articulated cylinder,

$$V_l = \sum_{q=1}^{N-1} l_q \cos(\phi_q - \phi_N)\dot{\phi}_q + l_N\dot{\phi}_N + U\sin\phi_N.$$

Moreover, as $x = \xi\cos\phi_N$, $(\partial/\partial x)$ can be replaced by $(\partial/\partial\xi)(1/\cos\phi_N)$ in equation (15), and by a Taylor series, $\cos^{-1}\phi_N \approx (1 - \frac{1}{2}\phi_N^2)^{-1} \approx 1 + \frac{1}{2}\phi_N^2$. The final expression for F_{nc} for the articulated system has been obtained by expanding the trigonometric functions via Taylor series expansions and integrating with respect to ξ; for $N = 2$ and $l_1 = l$, $l_2 = el$, this is

$$\begin{aligned} F_{nc} = {} & \tfrac{1}{2}\chi(1 - f)Mwl\ddot{\phi}_1[1 - \tfrac{1}{2}(\phi_2 - \phi_1)^2] - \chi(1 - f)MUl\dot{\phi}_1(1 + \phi_1\phi_2 - \tfrac{1}{2}\phi_1^2) \\ & + \tfrac{1}{2}\chi(1 - f)Mwl(\phi_1\dot{\phi}_1\dot{\phi}_2 - \phi_2\dot{\phi}_1\dot{\phi}_2 - \phi_1\dot{\phi}_1^2 + \phi_2\dot{\phi}_1^2) \\ & + \tfrac{1}{2}\chi(1 - f)Mewl\ddot{\phi}_2 + \tfrac{1}{2}\chi(1 - f)MUw\dot{\phi}_2(1 - \tfrac{1}{2}\phi_2^2) \\ & - \chi(1 - f)MUel(\dot{\phi}_2 + \tfrac{1}{2}\dot{\phi}_2\phi_2^2) - \chi(1 - f)MU^2(\phi_2 + \tfrac{1}{3}\phi_2^3). \end{aligned} \tag{16}$$

2.3.2. The hydrostatic pressure forces, F_{px} and F_{py}

By considering the hydrostatic pressure forces per unit length, F_{px} and F_{py}, due to the steady-state pressure p, it is noted that, with the assumption of linearity of the axial pressure gradient, one may write for the jth cylinder of the articulated system [11]:

$$(F_{px})_j = 0, \qquad (F_{py})_j = A(\mathrm{d}p/\mathrm{d}x)\tan\phi_j. \tag{17}$$

Furthermore, by assuming that lateral movement of the cylinder has negligible effect on the axial pressure distribution, one may write:

$$A\frac{\mathrm{d}p}{\mathrm{d}x} = -\tfrac{1}{2}\rho DU^2C_f\frac{D}{D_h} + \rho gA. \tag{18}$$

Hence, one obtains for the jth cylinder:

$$(F_{py})_j = \left(-\tfrac{1}{2}\rho DU^2C_f\frac{D}{D_h} + \rho gA\right)\tan\phi_j. \tag{19}$$

There will be an additional pressure force at each joint, related to curvature in continuously

flexible systems and equal to $pA[\partial^2 y/\partial x^2]$; for the articulated system, the corresponding terms are taken into account in the generalized forces.

By replacing $\tan \phi_j$ by its Taylor series approximation in equation (19), one obtains

$$(F_{py})_j = \left(-\tfrac{1}{2}\rho D U^2 C_f \frac{D}{D_h} + \rho g A \right)(\phi_j + \tfrac{1}{3}\phi_j^3). \tag{20}$$

2.3.3. Viscous hydrodynamic forces F_N and F_L

The viscous forces acting on long inclined cylinders (per unit length) have been formulated by Taylor [18]. They are given by

$$F_N = \tfrac{1}{2}\rho D U^2 (C_{dp} \sin^2 \phi + C_f \sin \phi), \qquad F_L = \tfrac{1}{2}\rho D U^2 C_f \cos \phi, \tag{21}$$

and they are in the $\mathbf{j}_1$- and $\mathbf{i}_1$-direction, respectively (see Figure 2). It has been shown that these formulae agree with the empirical results gathered by Hoerner [19], for which $C_{dp} = 1{\cdot}1$ and $C_f = 0{\cdot}02$.

However, for the purposes of this model, things are modified, e.g., by the fact that the instantaneous normal velocity is $v_{fj1}(\xi)$, which is the relative fluid-body velocity in the $\mathbf{j}_1$-direction, normal to the element, and which is given by equation (9). Hence, the expressions in equations (21) become

$$(F_N)_j = \tfrac{1}{2}\rho D C_{dp} \left[U \sin \phi_j + \sum_{q=1}^{j-1} l_q \cos(\phi_q - \phi_j)\dot{\phi}_q + \xi \dot{\phi}_j \right]^2$$

$$+ \tfrac{1}{2}\rho D U C_f \left[U \sin \phi_j + \sum_{q=1}^{j-1} l_q \cos(\phi_q - \phi_j)\dot{\phi}_q + \xi \dot{\phi}_j \right] \tag{22}$$

and

$$(F_L)_j = \tfrac{1}{2}\rho D U C_f \left[U \cos \phi_j - \sum_{q=1}^{j-1} l_q \sin(\phi_q - \phi_j)\dot{\phi}_q \right] \tag{23}$$

for the jth cylinder of the articulated system. In these equations, one may see that there are basically two kinds of terms: those related directly to lateral velocities, for instance $\xi\dot{\phi}_j$ (for $\dot{\phi}_j > 0$ and $\dot{\phi}_j < 0$ one should get F_N with opposite signs; i.e., always opposing motion); and those related to the approximating angles, such as $\sin^2 \phi_j$, the sign of which should be positive or negative, as ϕ_j is positive or negative. Tryantafyllou and Chryssostomidis [20] have shown that the term of the form $[U \sin \phi_1 + \xi\dot{\phi}_1]^2$, which is found in equation (22) for $(F_N)_1$, could be written as $[U \sin \phi_1 + \xi\dot{\phi}_1]|(U \sin \phi_1 + \xi\dot{\phi}_1)|$ directly; this formulation gives the same forces $(F_N)_j$ and $(F_L)_j$, $j = 1, 2$, as those obtained with the method just described.

By replacing the Taylor approximations for the trigonometric functions appearing in equations (22) and (23), and by taking into account the last paragraph, one obtains for the first and the second cylinder of the system, respectively, the following equations for the viscous forces $(F_N)_j$ and $(F_L)_j$:

$$(F_N)_1 = \tfrac{1}{2}\rho D U^2 C_{dp} \phi_1 |\phi_1| (1 - \tfrac{1}{3}\phi_1^2) + \tfrac{1}{2}\rho D U C_{dp} \xi (\dot{\phi}_1 |\dot{\phi}_1| + |\dot{\phi}_1| \dot{\phi}_1)(1 - \tfrac{1}{6}\phi_1^2)$$

$$+ \tfrac{1}{2}\rho D C_{dp} \xi^2 |\dot{\phi}_1| \dot{\phi}_1 + \tfrac{1}{2}\rho D U C_f [U\phi_1(1 - \tfrac{1}{6}\phi_1^2) + \xi\dot{\phi}_1], \tag{24}$$

$$(F_N)_2 = \tfrac{1}{2}\rho D C_{dp} l^2 \dot{\phi}_1 |\dot{\phi}_1| [1 - (\phi_2 - \phi_1)^2] + \tfrac{1}{2}\rho D U^2 C_{dp} \phi_2 |\phi_2| (1 - \tfrac{1}{3}\phi_2^2)$$
$$+ \tfrac{1}{2}\rho D U C_{dp} l [|\dot{\phi}_1| \phi_2 + \dot{\phi}_1 |\phi_2|][1 - \tfrac{1}{6}\phi_2^2 - \tfrac{1}{2}(\phi_2 - \phi_1)^2]$$
$$+ \tfrac{1}{2}\rho D U C_{dp} \xi (|\dot{\phi}_2| \phi_2 + \dot{\phi}_2 |\phi_2|)(1 - \tfrac{1}{6}\phi_2^2)$$
$$+ \tfrac{1}{2}\rho D C_{dp} l \xi [\dot{\phi}_1 |\dot{\phi}_2| + |\dot{\phi}_1| \dot{\phi}_2][1 - \tfrac{1}{2}(\phi_2 - \phi_1)^2] + \tfrac{1}{2}\rho D C_{dp} \xi^2 \dot{\phi}_2 |\dot{\phi}_2|$$
$$+ \tfrac{1}{2}\rho D U C_f [\xi \dot{\phi}_2 + U \phi_2 (1 - \tfrac{1}{6}\phi_2^2) + l \dot{\phi}_1 (1 - \tfrac{1}{2}(\phi_2 - \phi_1)^2)], \tag{25}$$

$$(F_L)_1 = \tfrac{1}{2}\rho D U^2 C_f (1 - \tfrac{1}{2}\phi_1^2), \tag{26}$$

$$(F_L)_2 = \tfrac{1}{2}\rho D U C_f [U(1 - \tfrac{1}{2}\phi_2^2) - l \dot{\phi}_1 (\phi_2 - \phi_1 - \tfrac{1}{6}(\phi_2 - \phi_1)^3)]. \tag{27}$$

2.4. THE GENERALIZED FORCES

The generalized forces Q_j, $j = 1, 2, \ldots, N$, associated with all the forces obtained in Section 2.3 may be determined by considering the virtual work δW_j associated with virtual displacements $\delta\phi_j$ in the generalized coordinates ϕ_j. Thus, the generalized force Q_j is defined via $\delta W_j = Q_j \delta\phi_j$. We proceed to determine the generalized force Q_1, associated with the generalized coordinate ϕ_1 and cylinder 1, which is denoted by $\delta W_{1,1}$ and is given by

$$\delta W_{1,1} = -\int_0^{l_1} (F_N)_1 \xi \delta\phi_1 \, d\xi + \int_0^{l_1} (F_{py})_1 \xi \delta\phi_1 \cos\phi_1 \, d\xi. \tag{28}$$

Similarly, the virtual work associated with the forces acting on the second cylinder, $\delta W_{1,2}$, due to a virtual displacement associated with $\delta\phi_1$, is given by

$$\delta W_{1,2} = -\int_0^{l_2} (F_N)_2 l_1 \delta\phi_1 \cos(\phi_2 - \phi_1) \, d\xi + \int_0^{l_2} (F_{py})_2 l_1 \delta\phi_1 \cos\phi_1 \, d\xi$$
$$+ \int_0^{l_2} (F_L)_2 l_1 \delta\phi_1 \sin(\phi_2 - \phi_1) \, d\xi - (\partial p/\partial x)_2 A_2 l_2 l_1 \delta\phi_1 \sin(\phi_2 - \phi_1); \tag{29}$$

and so on. The last term is that referred to in Section 2.3.2, below equation (19). The virtual work associated with the last cylinder will have the additional terms

$$\tfrac{1}{2}\rho D^2 U^2 C_b l_1 \delta\phi_1 \sin(\phi_N - \phi_1) + F_{nc} l_1 \delta\phi_1 \cos(\phi_N - \phi_1), \tag{30}$$

where C_b is the base drag coefficient, and F_{nc} has been discussed in Section 2.3.1.

Hence, the generalized force, Q_j, associated with the virtual displacement ϕ_j is

$$Q_j = -\int_0^{l_j} (F_N)_j \xi \, d\xi + \int_0^{l_j} (F_{py})_j \xi \cos\phi_j \, d\xi + \sum_{i=j+1}^{N} \left\{ -\int_0^{l_i} (F_N)_i l_j \cos(\phi_i - \phi_j) \, d\xi \right.$$
$$\left. + \int_0^{l_i} (F_{py})_i l_j \cos\phi_j \, d\xi + \int_0^{l_i} (F_L)_i l_j \sin(\phi_i - \phi_j) \, d\xi \right\} - F_{nc} l_j \cos(\phi_N - \phi_j)$$
$$- \sum_{i=j+1}^{N} (\partial p/\partial x)_i A_i l_i l_j \sin(\phi_i - \phi_j) + (\rho D^2 U^2 C_b/2) l_j \sin(\phi_N - \phi_j), \tag{31}$$

where $(F_N)_j$, $(F_L)_j$, $(F_{py})_j$ and F_{nc} are given by equations (22), (23), (20) and (16), respectively.

2.5. TRILINEAR AND CUBIC SPRING DESCRIPTION

Following the onset of flutter instability, the amplitude of oscillation will grow, resulting in impacting with the outer flow-containment cylinder. The interaction with the outer cylinder is assumed to be approximately trilinear, as shown in Figure 3. For contact at

the second articulation (lower end of the first cylinder) and denoting the displacement at the point by $\eta = l_1 \sin \phi_1$ and the contact stiffness by k_t, the force exerted by the trilinear spring may be expressed as

$$F_t(\eta) = k_t\{\eta - \tfrac{1}{2}[|\eta + \eta_g| - |\eta - \eta_g|]\},$$

where $\eta_g = l_1 \sin \phi_g$ is defined in Figure 3. Recalling that in the equations of motion we are dealing with moments and angles, rather than forces and displacements, the moment associated with the trilinear spring is

$$\mathscr{M}_t(\phi_1) = k_t l_1^2\{\sin \phi_1 - \tfrac{1}{2}[|\sin \phi_1 + \sin \phi_g| - |\sin \phi_1 - \sin \phi_g|]\}. \tag{32}$$

For analytical convenience [10], an alternative, cubic-spring approximation may be utilized instead of the trilinear one to model impacting with the outer cylinder. The force-displacement relationship in this case is

$$F_c(\eta) = k_c \eta^3,$$

and the moment-displacement relationship is

$$\mathscr{M}_c(\phi_1) = k_c l_1^2 \sin^3 \phi_1. \tag{33}$$

For the results presented in this paper, only the cubic spring has been used to model the impact.

2.6. DERIVATION OF THE EQUATIONS OF MOTION

The total kinetic energy of the system, T, is given by $T = T_s + T_f$, where T_s and T_f are given by equations (6) and (14), respectively. The potential energy, V_s, is associated only with the articulated system, and so with equation (7). The generalized and impact forces are given by equations (31) and (33).

Equations (6), (7), (14), (31) and (33) are substituted into Lagrange's equations

$$\frac{\mathrm{d}}{\mathrm{d}t}\left(\frac{\partial T}{\partial \dot{\phi}_j}\right) - \frac{\partial T}{\partial \phi_j} + \frac{\partial V}{\partial \phi_j} = Q_j, \quad j = 1, 2, \ldots, N, \tag{34}$$

where the dots denote differentiation with respect to time t, from which the equations of motion are obtained. These equations may be rendered non-dimensional with the

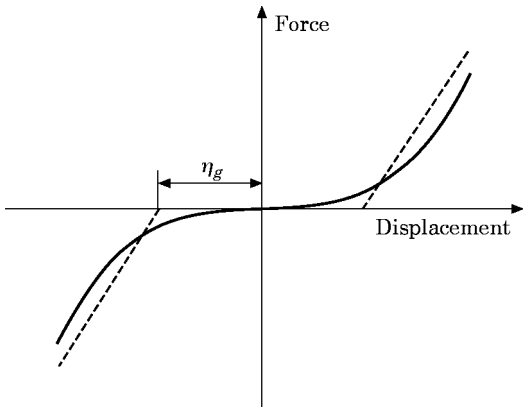

Figure 3. Force-displacement curves for the realistic trilinear-spring model (– – –) for impacting of the articulated system on the confining channel, and the cubic-spring idealization (——).

aid of the following dimensionless parameters:

$$\beta = \rho A/(\rho A + m), \quad \gamma = (m - \rho A)gL^2N/k, \quad u = (\rho ALN/k)^{1/2}U,$$
$$\epsilon = L/D, \quad l_N = el, \quad \lambda = w/l, \quad c = (4/\pi)C_d[\rho ALN/k]^{1/2},$$
$$c_f = 4C_f/\pi, \quad c_b = 4C_b/\pi, \quad h = D_h/D, \quad \tau = [(\rho A + m)L^3N/k]^{-1/2}t, \tag{35}$$

in which $L = \Sigma_{j=1}^{N} l_j$, and $l_1 = l_2 = \cdots = l_{N-1} = l$. For a system of two articulated cylinders ($N = 2$), the equations of motion in their final non-dimensional form are the following:

$$\begin{aligned}
&[1 + (\chi - 1)\beta][(\tfrac{1}{3} + e)\ddot{\phi}_1 + \tfrac{1}{2}e^2\ddot{\phi}_2] - \chi\beta e\ddot{\phi}_1(\phi_1 - \phi_2)^2 - \tfrac{1}{4}[1 + (\chi - 1)\beta]e^2\ddot{\phi}_2(\phi_1 - \phi_2)^2 \\
&\quad + \tfrac{1}{2}e^2\dot{\phi}_2^2[1 + (\chi - 1)\beta](\phi_1 - \phi_2) - \chi\beta\dot{\phi}_1(\dot{\phi}_2\phi_2 - \dot{\phi}_2\,\phi_1 - \tfrac{1}{2}\dot{\phi}_1\phi_2 + \tfrac{1}{2}\dot{\phi}_1\phi_1) \\
&\quad + \chi uN\sqrt{\beta}\dot{\phi}_2[e - \phi_2^2 + \phi_1\phi_2 - \tfrac{1}{4}\phi_1^2] - \chi u^2N^2\phi_1(1 - \tfrac{2}{3}\phi_1^2) + \tfrac{1}{2}(1 + 2e)N\gamma\phi_1(1 - \tfrac{1}{6}\phi_1^2) \\
&\quad + N^4(2\phi_1 - \phi_2) - \frac{\beta}{1 - 2\beta}N\gamma\phi_2^2\tfrac{1}{4}(\phi_2 - \phi_1) + \tfrac{1}{4}(2e + 1)u^2N\epsilon c_f h^{-1}(\phi_1 - \tfrac{1}{6}\phi_1^3 + \tfrac{1}{4}\phi_2^3 \\
&\quad - \tfrac{1}{4}\phi_1\phi_2^2) + \tfrac{1}{2}u^2N^2c_b(\phi_1 - \phi_2 + \tfrac{1}{6}\phi_2^3 - \tfrac{1}{2}\phi_1\phi_2^2 + \tfrac{1}{2}\,\phi_1^2\phi_2 - \tfrac{1}{6}\phi_1^3) \\
&\quad - \tfrac{1}{2}(1 - f)\chi\beta\lambda\ddot{\phi}_1[1 - (\phi_2 - \phi_1)^2] - \tfrac{1}{2}(1 - f)\chi e\beta\lambda\ddot{\phi}_2[1 - \tfrac{1}{2}(\phi_2 - \phi_1)^2] \\
&\quad - \tfrac{1}{2}(1 - f)\chi\beta\lambda[\phi_1\dot{\phi}_1\dot{\phi}_2 - \dot{\phi}_1\dot{\phi}_2\phi_2 - \phi_1\dot{\phi}_1^2 + \dot{\phi}_1^2\phi_2] - \tfrac{1}{2}(1 - f)\chi uN\sqrt{\beta}\lambda\dot{\phi}_2[1 - \tfrac{1}{2}\,\phi_2^2] \\
&\quad + (1 - f)\chi uN\sqrt{\beta}e\dot{\phi}_2(1 - \tfrac{1}{2}\phi_1^2 + \phi_1\phi_2) + (1 - f)\chi uN\sqrt{\beta}\dot{\phi}_1(1 + \phi_1\phi_2 - \tfrac{1}{2}\dot{\phi}_1\phi_2^2 \\
&\quad + \phi_1\dot{\phi}_1\phi_2) + (1 - f)\chi u^2N^2\phi_2(1 - \tfrac{1}{6}\phi_2^2 + \phi_1\phi_2) - (1 - f)\chi u^2N^2\tfrac{1}{2}\phi_1^2\phi_2 \\
&\quad + \tfrac{1}{4}u^2N\epsilon c|\phi_1|\phi_1 + \tfrac{3}{8}\epsilon c\frac{\beta}{N}|\dot{\phi}_1|\dot{\phi}_1 + \tfrac{1}{6}u\epsilon c\sqrt{\beta}[|\dot{\phi}_1|\phi_1 + \dot{\phi}_1|\phi_1|] + \tfrac{1}{6}\frac{1}{N}\epsilon c\beta e^3\dot{\phi}_2|\dot{\phi}_2| \\
&\quad + u^2N\epsilon c\,\tfrac{1}{2}\,e\,\phi_2|\phi_2| + \epsilon c\beta e^2\frac{1}{N}\tfrac{1}{4}[\dot{\phi}_1|\dot{\phi}_2| + |\dot{\phi}_1|\dot{\phi}_2] + \tfrac{1}{4}e^2u\epsilon c\sqrt{\beta}[|\dot{\phi}_2|\phi_2 + \dot{\phi}_2|\phi_2|] \\
&\quad + \tfrac{1}{2}u\epsilon c\sqrt{\beta}e[|\dot{\phi}_1|\phi_2 + \dot{\phi}_1|\phi_2|] + \tfrac{1}{6}(3e + 1)\epsilon c_f u\sqrt{\beta}\dot{\phi}_1 + \tfrac{1}{4}(2e + 1)u^2N\epsilon c_f[\phi_1 - \tfrac{1}{6}\phi_1^3] \\
&\quad + \tfrac{1}{4}\epsilon c_f\sqrt{\beta}ue^2\dot{\phi}_2[1 - \tfrac{1}{2}(\phi_2 - \phi_1)^2] + \mathscr{M}_c = 0, \\
&[1 + (\chi - 1)\beta](\tfrac{1}{3}e^3\ddot{\phi}_2 + \tfrac{1}{2}e^2\ddot{\phi}_1) - [1 + (\chi - 1)\beta]\tfrac{1}{4}e^2(\phi_1 - \phi_2)^2\ddot{\phi}_1 \\
&\quad + \tfrac{1}{2}e^2[1 + (\chi - 1)\beta]\dot{\phi}_1^2(\phi_2 - \phi_1) - \chi\beta e(\phi_1 - \phi_2)\dot{\phi}_1^2 - \chi u^2N^2e(1 - \tfrac{2}{3}\phi_2^2)\phi_2 \\
&\quad - \chi uNe\sqrt{\beta}\dot{\phi}_1(1 - 2\phi_2^2 - \tfrac{1}{2}\phi_1^2 + 2\phi_1\phi_2) + N\gamma\tfrac{1}{2}e^2(\phi_2 - \tfrac{1}{6}\phi_2^3) + N^4(\phi_2 - \phi_1) \\
&\quad + \epsilon c\beta e^2\frac{1}{N}\tfrac{1}{4}\dot{\phi}_1|\dot{\phi}_1| + \epsilon c\beta e^4\frac{1}{N}\tfrac{1}{8}\dot{\phi}_2|\dot{\phi}_2| + \epsilon c\beta e^3\frac{1}{N}\tfrac{1}{6}[|\dot{\phi}_1|\dot{\phi}_2 + \dot{\phi}_1|\dot{\phi}_2|] \\
&\quad + u^2\epsilon cNe^2\tfrac{1}{4}\phi_2|\phi_2| + u\epsilon c\sqrt{\beta}e^3\tfrac{1}{6}[|\dot{\phi}_2|\phi_2 + \dot{\phi}_2|\phi_2|] + u\epsilon c\sqrt{\beta}e^2\tfrac{1}{4}[|\dot{\phi}_1|\phi_2 + \dot{\phi}_1|\phi_2|] \\
&\quad + \tfrac{1}{4}u^2N\epsilon c_f e^2(1 + h^{-1})(\phi_2 - \tfrac{1}{6}\phi_2^3) - \tfrac{1}{2}\chi\beta(1 - f)e\lambda\ddot{\phi}_1[1 - \tfrac{1}{2}(\phi_2 - \phi_1)^2] \\
&\quad - \tfrac{1}{2}\chi\beta e\lambda(1 - f)(\dot{\phi}_1^2\phi_2 - \phi_1\dot{\phi}_1^2 - \dot{\phi}_1\dot{\phi}_2\phi_2 + \phi_1\dot{\phi}_1\dot{\phi}_2) - \tfrac{1}{2}(1 - f)\chi\beta\lambda e^2\ddot{\phi}_2 \\
&\quad + \tfrac{1}{6}\sqrt{\beta}u\epsilon c_f e^3\dot{\phi}_2 + \tfrac{1}{4}\sqrt{\beta}\epsilon c_f ue^2\dot{\phi}_1[1 - \tfrac{1}{2}(\phi_2 - \phi_1)^2] - \tfrac{1}{2}(1 - f)e\chi uN\sqrt{\beta}\lambda\dot{\phi}_2(1 - \tfrac{1}{2}\phi_2^2) \\
&\quad + \chi(1 - f)euN\sqrt{\beta}\dot{\phi}_1(1 - \tfrac{1}{2}\phi_1^2 + \phi_1\phi_2) + (1 - f)\chi uNe^2\sqrt{\beta}\dot{\phi}_2(1 + \tfrac{1}{2}\phi_2^2) \\
&\quad + e(1 - f)\chi u^2N^2(\phi_2 + \tfrac{1}{3}\phi_2^3) = 0.
\end{aligned} \tag{36}$$

Equations (36) were obtained for the non-linear model, in which the non-linearities to $O(\epsilon^3)$, where displacements are of $O(\epsilon)$, were introduced through Taylor approximations; this will henceforth be referred to as *Model 1*. A much simpler model is the "linearized"

one, to be referred to as *Model 2*, in which the equations, apart from the impact force which is modelled by a cubic spring, are linearized. The linearized model has been studied previously by Païdoussis and Botez [10, 11]. The results from the two models will be compared for two cases, by varying only two parameters, and keeping the other parameters constant, as discussed in Section 3.

Solutions of the equations of motion were obtained by using a fourth-order Runge–Kutta integration algorithm, with a time step $\delta\tau = 0{\cdot}01$. When this time step was changed to $\delta\tau = 0{\cdot}001$, the same results were obtained to the fourth significant figure.

3. THE SYSTEMS TO BE INVESTIGATED

The dynamics of two systems will be examined in this paper, in order to assess similarities and differences between the non-linear *Model 1* and the simplified, essentially linearized *Model 2*. Most system parameters will be the same in the two systems, while two will be varied, thus defining the two systems, which will hereafter be referred to as Case 1 and Case 2.

The constant parameters are

$$\epsilon = 10, \quad e = 0{\cdot}5, \quad \beta = 0{\cdot}4, \quad \gamma = 10, \quad \epsilon c_f = 0{\cdot}25, \quad c_b = 0{\cdot}1, \quad \kappa_c = 5 \times 10^5,$$

while h and f will be varied; h gives a measure of the annular gap width between the articulated cylinder system and the outer pipe, and f is the non-dimensional parameter associated with the free-end shape. For the two cases to be studied, these parameters are

$$\text{Case 1:} \quad h = 0{\cdot}2 \quad \text{and} \quad f = 0{\cdot}4; \qquad \text{Case 2:} \quad h = 0{\cdot}5 \quad \text{and} \quad f = 0. \tag{37}$$

It is recalled that c is the damping in zero flow and is controlled by the tightness of the annulus. It is not an independent parameter, but depends on h [21]. For Case 1 where $h = 0{\cdot}2$, $c = 0{\cdot}79$; while for Case 2 where $h = 0{\cdot}5$, $c = 0{\cdot}39$. It may be of interest to know, approximately, the shape of the paraboloidal ogival end corresponding to the value of f selected. For Case 1, where $f = 0{\cdot}4$, $\lambda = w/l = 0{\cdot}78/7{\cdot}75$; this, in terms of the diameter D, corresponds to $w/D = 0{\cdot}78/1{\cdot}55 = 0{\cdot}50$, where the dimensions could be in cm for a laboratory experiment. For Case 2, where $f = 0$, the value of λ and w are: $0 \leqslant \lambda \leqslant 0{\cdot}025$ and $0 \leqslant w/D < 0{\cdot}12$. See also Appendix A.

The dynamics of Cases 1 and 2 will be presented and discussed in detail according to *Models 1* and *2*, in Sections 4 and 5, respectively. Cases with other values of f, but the same two values of h will be discussed in Section 6.

4. THE DYNAMICS OF CASE 1

4.1. CASE 1 WITH *MODEL 1*

For this and most other cases treated in this paper, the dynamical behaviour is characterized in terms of the angular displacement $\phi_1(\tau)$ and the corresponding velocity $\dot{\phi}_1(\tau)$. The character of the motion nevertheless is the same for the whole system: i.e., if the motion of the first cylinder is quasi-periodic, periodic or chaotic, so is that of the second one.

We now consider the equations of motion (36) for Case 1 ($h = 0{\cdot}2, f = 0{\cdot}4$). By graphing the maximum displacement of the first cylinder, $\phi_{1\max}$, as a function of u, a bifurcation diagram is constructed, as shown in Figure 4 for $u > u_{fl} = 2{\cdot}45$. The dynamics associated with this bifurcation diagram is clarified via phase-phase portraits in Figure 5.

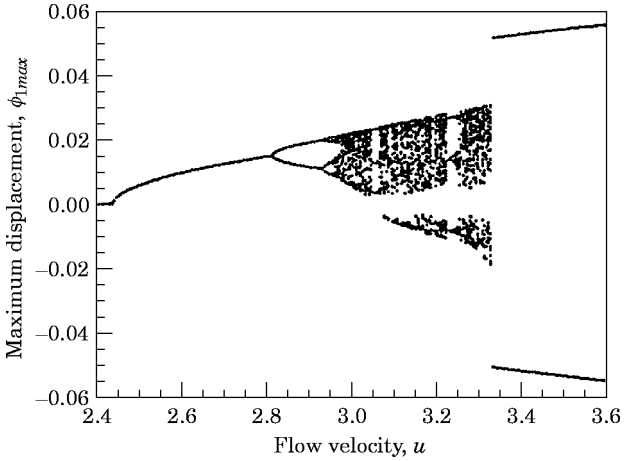

Figure 4. Bifurcation diagram showing $\phi_{1\max}$ versus u, obtained with the first model; Case 1: $h = 0{\cdot}2$ and $f = 0{\cdot}4$.

There exists a symmetric stable limit cycle which develops after the Hopf bifurcation (onset of flutter) which occurs for $u_{fl} = 2{\cdot}45$ (see Figure 4). The symmetry of the limit cycle is lost by a symmetry-breaking pitchfork bifurcation at $u_{pf} = 2{\cdot}805$ (Figure 4), where the two branches are obtained with different-sign initial conditions; the asymmetry of the limit cycle may be seen in Figure 5(a) for $u = 2{\cdot}85$.

For $u > u_{p2} = 2{\cdot}929$ (where the subscript stands for *period*-2), a cascade of period-doubling bifurcations occurs; Figure 5(b, c) shows period-2 and period-4 motions for $u = 2{\cdot}95$ and $u = 2{\cdot}955$, respectively. For $u > u_{ch} = 2{\cdot}959$ approximately, the bifurcation diagram shows that the motion might be chaotic; this is reinforced by the phase-plane diagram of Figure 5(d), for $u = 3$. The Feigenbaum number is calculated for the period-doubling bifurcations shown in Figure 5(a–c), with thresholds at $u_{p2} = u_2 = 2{\cdot}929$ (period-2 motion), $u_4 = 2{\cdot}952$ (period-4 motion), and $u_8 = 2{\cdot}957$ period-8 motion, not shown). They give Fei $= 4{\cdot}6$, which is very close to the ideal Feigenbaum number

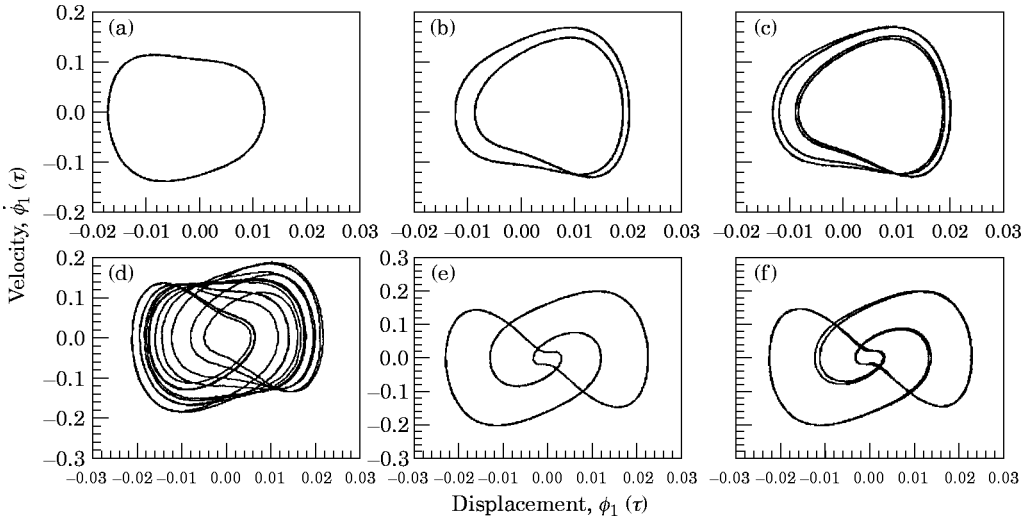

Figure 5. Phase-plane plots of $\dot{\phi}_1(\tau)$ versus $\phi_1(\tau)$ at (a) $u = 2{\cdot}85$, (b) $u = 2{\cdot}95$, (c) $u = 2{\cdot}955$, (d) $u = 3$, (e) $u = 3{\cdot}06$, and (f) $u = 3{\cdot}062$, obtained within the first model; Case 1: $h = 0{\cdot}2$ and $f = 0{\cdot}4$.

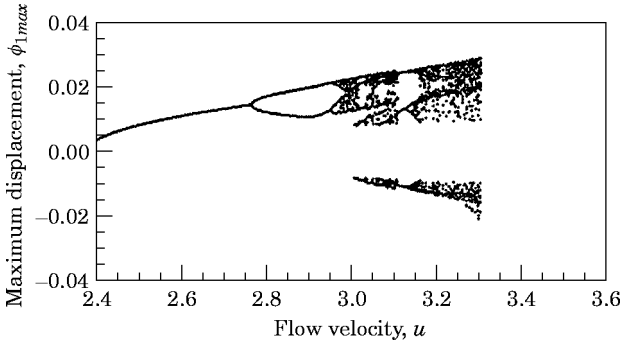

Figure 6. Bifurcation diagram showing $\phi_{1\max}$ versus u, obtained with the second model; Case 1: $h = 0{\cdot}2$ and $f = 0{\cdot}4$.

$\text{Fei}_{\text{ideal}} = 4{\cdot}6692$. Apart from appearance, it is important to verify that period-doubling does indeed occur in the aforementioned sequence. Hence, the frequency for the motions in Figure 5(a–c) was calculated from time traces and power spectra. The frequency of (a) period-1 motion is $f_1 = 1{\cdot}47$ for $u = 2{\cdot}85$; (b) period-2 motion is $f_2 = f_1/2$ for $u = 2{\cdot}95$; and (c) period-4 motion is $f_4 = f_1/4$ for $u = 2{\cdot}955$.

Beyond the initial occurrence of chaos there exist a number of periodic windows. Thus, as ascertained from time traces and power spectra, for $u = 3{\cdot}0456$–$3{\cdot}0605$ the motion of the system is periodic with period $T = 2{\cdot}275$, while for $u = 3{\cdot}0606$–$3{\cdot}0622$ it has undergone a period-doubling (to period $T = 4{\cdot}55$) with respect to the previous motion. These motions are shown in Figure 5(e, f) for (e) $u = 3{\cdot}06$ and (f) $u = 3{\cdot}062$, respectively. On the bifurcation diagram (when blown up), these periodic windows appear to be associated with period-3 and period-6 motions, as they are represented through three and six points, respectively. For $u = 3{\cdot}0622$–$3{\cdot}0623$, two more period-doublings occur. Thus, a second cascade of period-doubling bifurcations has occurred, leading to chaotic motions in the range $u = 3{\cdot}0624$–$3{\cdot}223$. Other periodic windows occur for higher flow velocities: for $u = 3{\cdot}224$–$3{\cdot}241$, period-1 with $T = 1{\cdot}2$; for $u = 3{\cdot}242$–$3{\cdot}243$, period-2 with $T = 2{\cdot}4$. Once again, for a small range of flow velocities, $u = 3{\cdot}243$–$3{\cdot}244$, period-4 and period-8 motions occur, which represent in fact the third cascade of period-doubling bifurcations in the bifurcation diagram, leading again to chaotic motions. For $u > 3{\cdot}3$, the motion of the system reduces to fixed points, as seen in Figure 4.

The route to chaos for this case may be summarized for increasing flow velocities, as follows: (1) period-doubling bifurcations leading to chaos; (2) a second cascade of period-doubling bifurcations and chaos, (3) again, period-doubling bifurcations followed by chaos; and finally, (4) fixed points. Therefore, this is an unusual case, with three sequential period-doubling bifurcation cascades.

4.2. CASE 1 WITH *MODEL 2*

Figures 6 and 7 show the bifurcation diagram and the phase-plane plots for the first cylinder in this system, for flow velocities u higher than the critical flow velocity at which flutter occurs via a Hopf bifurcation ($u_{fl} = 2{\cdot}39$); the dynamical behaviour is clarified via the phase-plane portraits of Figure 7.

The symmetric stable limit cycle, which develops after the Hopf bifurcation at $u_{fl} = 2{\cdot}39$ (not shown), suffers a symmetry-breaking pitchfork bifurcation at $u_{pf} = 2{\cdot}767$, the first bifurcation shown in Figure 6, where the two branches are obtained with opposite-sign initial conditions. The asymmetry of the limit cycle may be observed on Figure 7(a), for $u = 2{\cdot}85$. For $u > u_{p2} = 2{\cdot}952$, a cascade of period-doubling bifurcations occurs;

Figure 7(b, c) shows period-2 and period-4 motions for (b) $u = 2{\cdot}965$ and (c) $u = 2{\cdot}972$. Figure 7(d) shows chaotic motion for $u = 2{\cdot}975$. The period-doubling bifurcations have the following thresholds: $u_2 = 2{\cdot}952$ (period-2 motion), $u_4 = 2{\cdot}97$ (period-4 motion), and $u_8 = 2{\cdot}974$ (period-8 motion). They give Fei $= 4{\cdot}50$, which is close to the ideal value. The frequency of the period-1 motion is $f_1 = 1{\cdot}17$ for $u = 2{\cdot}85$, while for the period-2 motion it is $f_2 = f_1/2$ for $u = 2{\cdot}952$.

A periodic window appears for $u = 2{\cdot}9789$–$2{\cdot}9812$, as shown in Figure 7(e) for $u = 2{\cdot}98$. By analyzing the time traces and the power spectra for $u_1 = 2{\cdot}9789$, the fundamental frequency $f = 0{\cdot}39$ may be calculated. Since the motion is basically of period-3 form, the frequency here is approximately 1/3 that in Figure 7(a). For $u_2 = 2{\cdot}9807$, $f = 0{\cdot}195$ is obtained, so that this motion has undergone a period-doubling with respect to the previous periodic motion. For $u_3 = 2{\cdot}9811$ the motion undergoes a further period-doubling, followed by yet another for $u_4 = 2{\cdot}98121$; for higher flow velocities the motion of the system becomes chaotic. The Feigenbaum number corresponding to the last period-doubling sequence is Fei $\simeq 3{\cdot}64$, not close to the ideal $\text{Fei}_{\text{ideal}} = 4{\cdot}6692$. For $u = 3$, another periodic window appears, as illustrated in Figure 7(f). Then, for $u > 3$, a new cascade (the third one) of period-doublings occurs, for $u = 3{\cdot}11$–$3{\cdot}143$, which is qualitatively the same as the second one ($u = 2{\cdot}9789$–$2{\cdot}9812$).

The chaotic nature of the motion was confirmed via power spectra and time traces. Samples are shown in Figure 8, for two flow velocities, (a) $u = 2{\cdot}975$ and (b) $u = 3{\cdot}2$, confirming that the system is in fact undergoing chaotic oscillations. For the same values of u, the Poincaré sections were constructed in Figure 9, and they too were found to have the characteristics of chaotic motion, as expected.

Thus, for *Model 2* also, chaos appears and recurs through three period-doubling sequences as u is increased (Figure 6).

4.3. DISCUSSION

A more general discussion of the comparison of the dynamical behaviour according to Models 1 and 2 is carried out in Section 6. However, from the foregoing and specifically for Case 1, it is clear that the results are qualitatively similar. By comparing the bifurcation

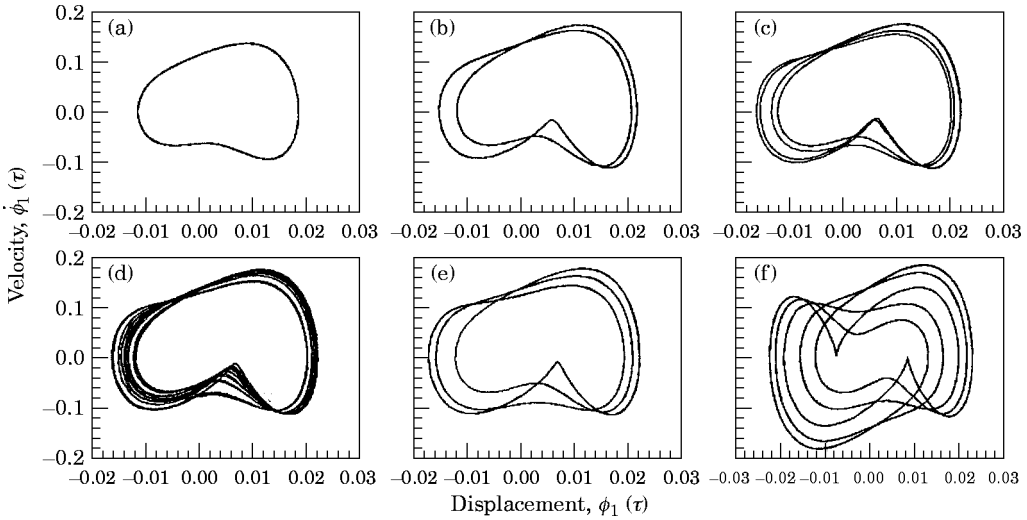

Figure 7. Phase-plane plots of $\dot{\phi}_1(\tau)$ versus $\phi_1(\tau)$ at (a) $u = 2{\cdot}85$; (b) $u = 2{\cdot}965$; (c) $u = 2{\cdot}972$; (d) $u = 2{\cdot}975$; (e) $u = 2{\cdot}98$ and (f) $u = 3$ obtained with the second model; Case 1: $h = 0{\cdot}2$ and $f = 0{\cdot}4$.

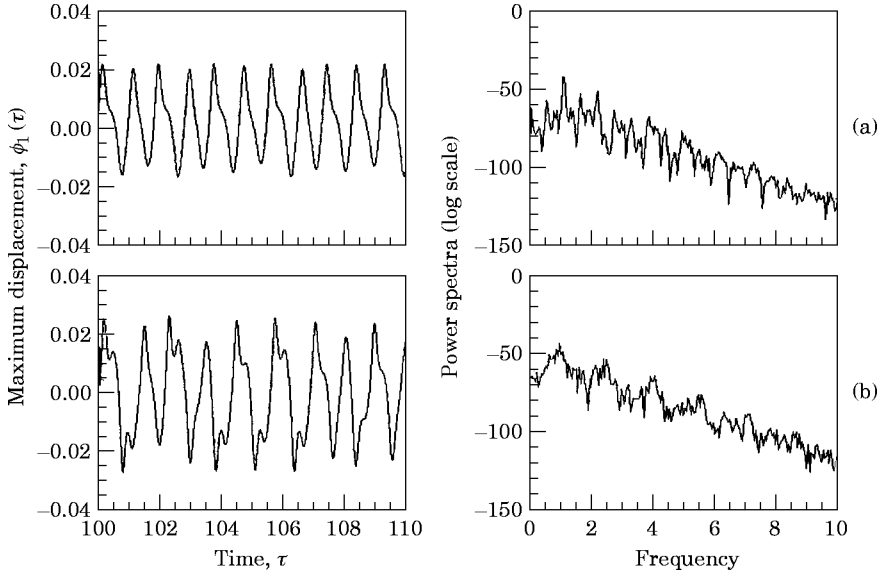

Figure 8. Time traces of $\phi_1(\tau)$ and logarithmic power spectra plotted in dimensionless time, τ, and the corresponding dimensionless frequency, obtained with the second model, for Case 1: $h = 0{\cdot}2$ and $f = 0{\cdot}4$, for (a) $u = 2{\cdot}975$ and (b) $u = 3{\cdot}2$.

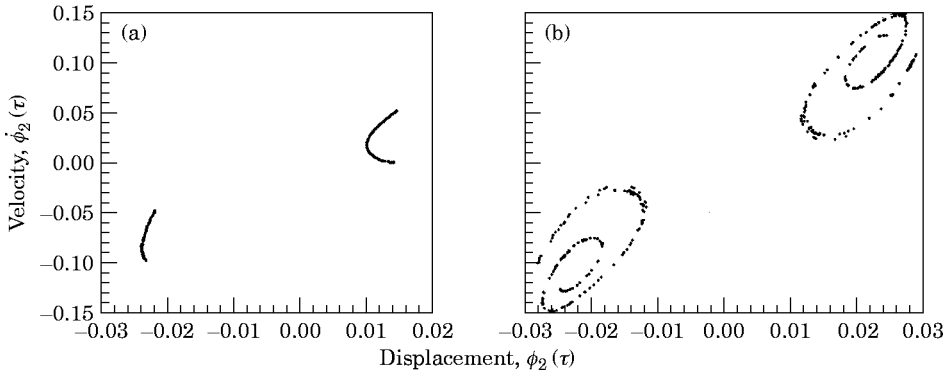

Figure 9. Poincaré sections of $\dot{\phi}_2(\tau)$ versus $\phi_2(\tau)$ when $\dot{\phi}_1(\tau) = 0$ for (a) $u = 2{\cdot}975$ and (b) $u = 3{\cdot}2$, obtained with the second model, for Case 1: $h = 0{\cdot}2$ and $f = 0{\cdot}4$.

diagrams for this case (Figures 4 and 6), as well as the corresponding phase plane portraits, power spectra and Poincaré sections for the two models (not all of which are included in this paper, for brevity), it may be concluded that the route to chaos is the same, namely through three period-doubling sequences, but differences in the quantitative sense do exist, as expected. For higher u, the motion of the system remains chaotic according to *Model 2*, while it reduces to a fixed point according to *Model 1*.

In Table 1, the critical flow velocities u_{fl}, u_{pf}, u_{p2}, and u_{ch} corresponding to u for which

TABLE 1

Case 1 *for Model* 1 *and Model* 2

	u_{fl}	u_{pf}	u_{p2}	u_{ch}	$\phi_{1\max}$ $(u = u_{fl})$	$\phi_{1\max}$ $(u = u_{pf})$	f_1 $(u = u_{fl})$	f_1 $(u = u_{pf})$
Model 1	2·45	2·805	2·929	2·959	0·002	0·0144	1·27	1·47
Model 2	2·39	2·767	2·952	2·975	0·002	0·0146	1·02	1·17

flutter, a pitchfork bifurcation, period-2 and chaotic motions occur, the maximum displacements for the first cylinder, $\phi_{1\max}$, and the fundamental frequencies f_1, are calculated for u_{fl}, and u_{pf}. A quantitative comparison is done for the two models, by considering $diff = |Model\ 1 - Model\ 2|/Model\ 1$, which is calculated for each of the parameters described above. This difference, *diff*, has been found to be between 0·5 and 2·4% for u, between 0 and 1·4% for $\phi_{1\max}$, and between 19·7 and 20·4% for f_1.

5. THE DYNAMICS OF CASE 2

5.1. CASE 2 WITH *MODEL 1*

In this case, a flutter instability occurs for $u_{fl} = 4{\cdot}65$. Physically, the annular space in this case is wider than in Case 1, and the free end is blunter; both tend to make u_{fl} higher than in Case 1. Figure 10 shows two bifurcation diagrams for motions of the first cylinder in the system, for flow velocities above the critical for which a Hopf bifurcation occurs ($u > u_{fl} = 4{\cdot}65$): Figure 10(a) for $5 < u < 8{\cdot}50$, and Figure 10(b) for $8 < u < 8{\cdot}30$ on an expanded scale.

The behaviour of the system is seen much better on the phase-plane portraits of Figure 11. Symmetric limit-cycle motions around the origin occur for $4{\cdot}65 < u < 6{\cdot}94$, represented on the bifurcation diagram in Figure 10(a) through a single point. For $6{\cdot}95 < u < 8{\cdot}09$ approximately, a "symmetric" periodic motion develops, which is shown in Figure 11(a) for $u = 7{\cdot}50$; it looks as if it develops around two symmetric points: for $\dot{\phi}_1 = 0$, $\phi_1 = \pm 0{\cdot}018$. For $8{\cdot}10 < u < 8{\cdot}18$, a periodic motion, locally looking like period-2 motion, occurs around the same two points, remaining always symmetric with respect to the origin, as seen in Figure 11(b) for $u = 8{\cdot}15$. The periodic motion evolves into a form locally looking like period-3 motion, for $8{\cdot}19 < u < 8{\cdot}225$, around the same pair of points, as seen in Figure 11(c) for $u = 8{\cdot}20$. The dominant frequencies of the system are calculated for the same flow velocities, as for those in the phase-plane portraits of Figure 11(a, b, c). Thus, for (a) $u = 7{\cdot}50$, the fundamental frequency is $f_1 = 0{\cdot}59$, for (b) $u = 8{\cdot}15$, $f_2 = f_1/2 = 0{\cdot}293$, while for (c) $u = 8{\cdot}20$, $f_3 = f_1/3$. Thus, for increasing flow velocity, the system has a period-1, 2, and 3 motion; it finally becomes chaotic for $u = 8{\cdot}25$, as shown in Figure 11(d), in which the chaotic motion of the system develops around one of the aforementioned symmetric points on either side of the origin. (Slightly chaotic motions around the same two points were found to exist also for $8{\cdot}185 < u < 8{\cdot}190$.)

Although chaotic motion around only one of the two symmetric points ($\phi_1 \approx -0{\cdot}018$ and $\dot{\phi}_1 = 0$) is observed in Figure 11(e) for $u = 8{\cdot}26$, it can occur around either one, depending on the initial conditions, as shown in Figure 12. Small-scale chaotic motions in Figure 12(a, b, c) are observed for (a) $u = 8{\cdot}25$ and (b, c) $u = 8{\cdot}26$. Figure 12(b) shows the chaotic motion of the system around one of the two symmetric points, while Figure 12(c) shows it around the other one; these were obtained with opposite-sign initial conditions, $\dot{\phi}_1 = \pm 0{\cdot}1$.

For higher flow velocities, a reverse period-doubling cascade takes place, for which a period-four motion may be observed for $u = 8{\cdot}264$ (not shown); a period-2 motion is presented in Figure 11(f) for $u = 8{\cdot}27$, still detached from its mirror image around the other point, which is followed by a reversion to period 1 motion for $u = 8{\cdot}274$ (not shown). This reverse period-doubling cascade was verified by the frequencies for each periodic motion: for $u = 8{\cdot}264$, the fundamental frequency is $f_1 = 0{\cdot}34$; for $u = 8{\cdot}27$, $f_2 = 0{\cdot}68 = 2f_1$; while for $u = 8{\cdot}274$, $f_3 = 4f_1$. The motion eventually reduces to a fixed point for $u > 8{\cdot}40$.

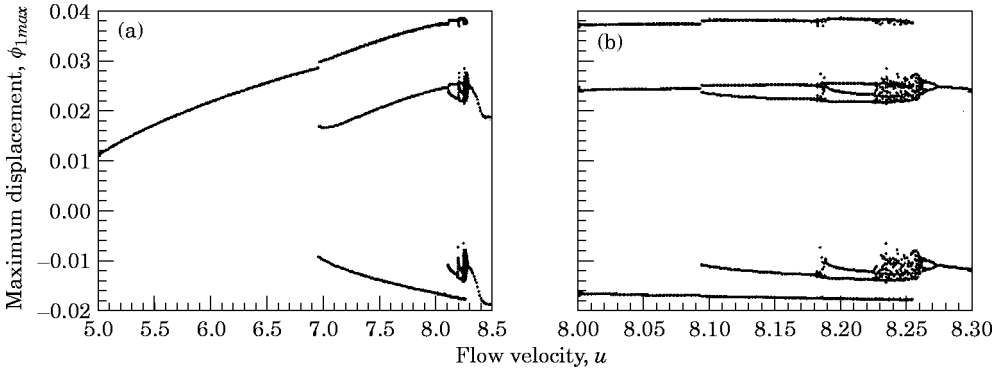

Figure 10. Bifurcation diagram showing ϕ_{1max} versus u, obtained with the first model, for Case 2: $h = 0{\cdot}5$ and $f = 0$; for (a) $5 < u < 8{\cdot}5$ and (b) $8 < u < 8{\cdot}30$.

Poincaré sections of $\dot{\phi}_2$ versus ϕ_2 for $\dot{\phi}_1 = 0$ have been constructed for some values of flow velocity and some are presented in Figure 13: for (a) $u = 8{\cdot}20$, showing many points and verifying the periodic nature of the motion; for (b) $u = 8{\cdot}25$ and (c) $u = 8{\cdot}26$, showing the chaotic nature of the motion for these flow velocities. These figures were constructed with 10 000 time steps.

Figure 14 shows the time traces and the power spectra for this system, for three different flow velocities, u: the motion of the system is seen clearly to be (a, b) periodic for $u = 8{\cdot}20$, and (c, d) chaotic for $u = 8.25$, as well as for (e, f) $u = 8{\cdot}26$.

Thus, this case displays rich and unusual dynamical behaviour. Chaos arises around two symmetric points, through periodic motions, progressing from period-1, to 2 and 3; then a reverse period-doubling cascade takes place, back to period-1 motion; and finally the motion reduces to fixed points.

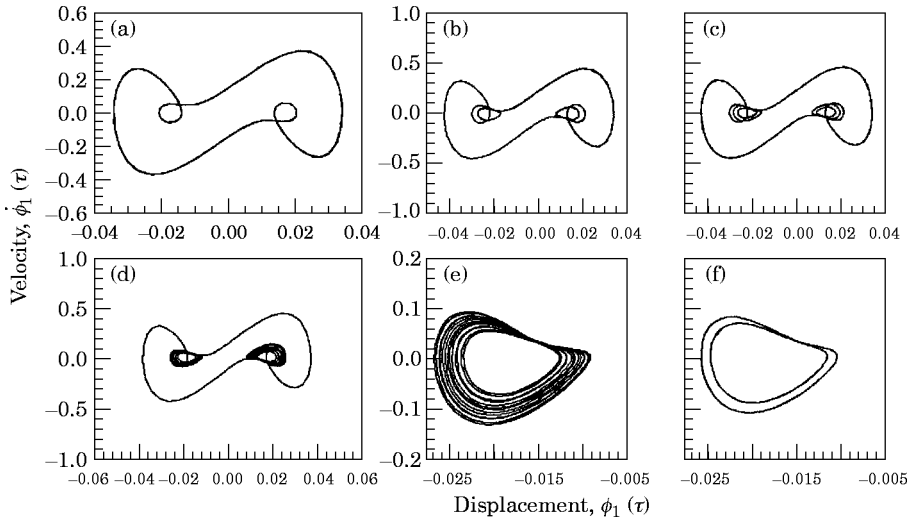

Figure 11. Phase-plane plots of $\dot{\phi}_1(\tau)$ versus $\phi_1(\tau)$ at (a) $u = 7{\cdot}5$, (b) $u = 8{\cdot}15$, (c) $u = 8{\cdot}20$, (d) $u = 8{\cdot}25$, (e) $u = 8.26$ and (f) $u = 8{\cdot}27$ obtained with the first model, for Case 2: $h = 0{\cdot}5$ and $f = 0$.

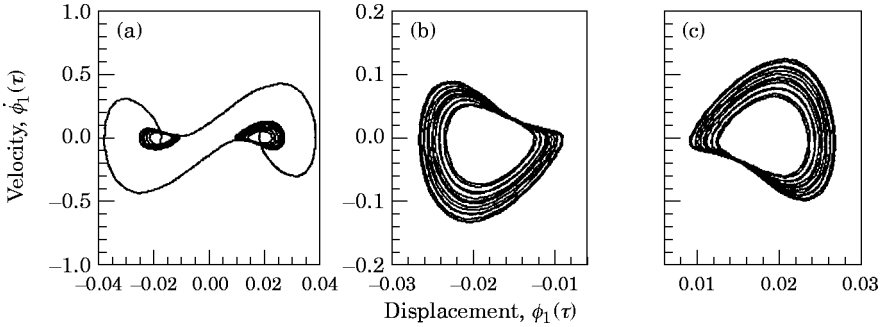

Figure 12. Phase-plane plots of $\dot{\phi}_1(\tau)$ versus $\phi_1(\tau)$ at (a) $u = 8{\cdot}25$ for $\dot{\phi}_1(\tau) = 0{\cdot}1$ or $\dot{\phi}_1(\tau) = -0{\cdot}1$, at (b) $u = 8{\cdot}26$ and $\dot{\phi}_1(\tau) = 0{\cdot}1$, and (c) $u = 8{\cdot}26$ and $\dot{\phi}_1(\tau) = -0{\cdot}1$, obtained with the first model, for Case 2: $h = 0{\cdot}5$ and $f = 0$.

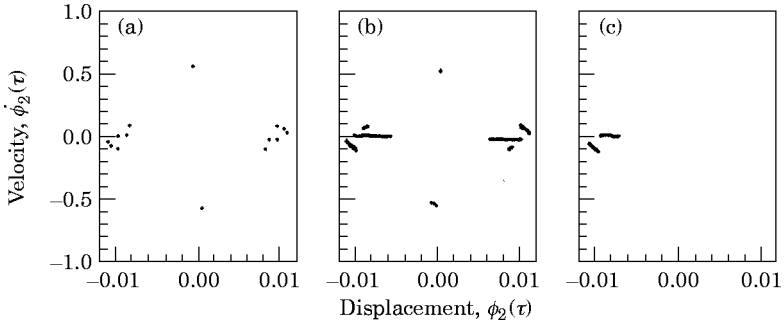

Figure 13. Poincaré sections of $\dot{\phi}_2(\tau)$ versus $\phi_2(\tau)$, when $\dot{\phi}_1(\tau) = 0$ for (a) $u = 8{\cdot}20$, (b) $u = 8{\cdot}25$ and (c) $u = 8{\cdot}26$, obtained with the first model, for Case 2: $h = 0{\cdot}5$ and $f = 0$.

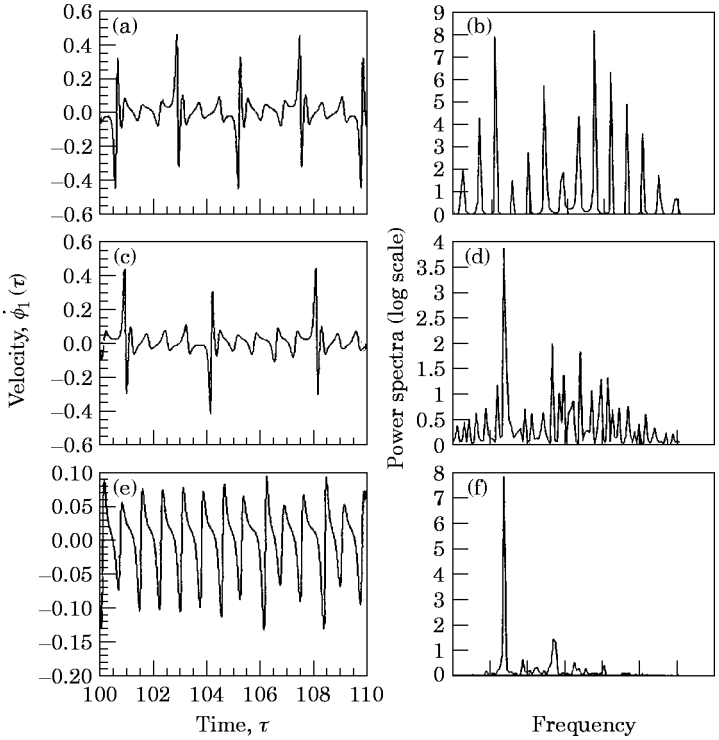

Figure 14. Time traces (a, c, e) of $\dot{\phi}_1(\tau)$ and linear power spectra (b, d, f) plotted in dimensionless time, τ, and the corresponding dimensionless frequency, obtained with the first model, for Case 2: $h = 0{\cdot}5$ and $f = 0$, for (a, b) $u = 8{\cdot}20$, (c, d) $u = 8{\cdot}25$ and (e, f) $u = 8{\cdot}26$.

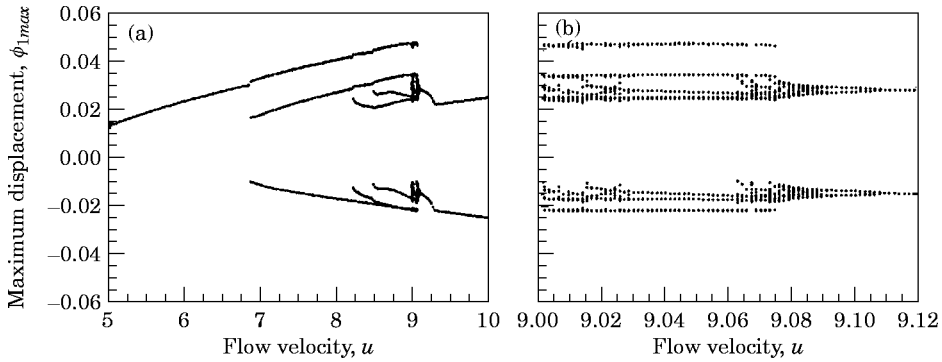

Figure 15. Bifurcation diagram showing $\phi_{1\max}$ versus u, obtained with the second model, for Case 2: $h = 0{\cdot}5$ and $f = 0$; for (a) $5 < u < 10$ and (b) $9 < u < 9{\cdot}12$.

5.2. CASE 2 WITH *MODEL 2*

Figures 15 and 16 show bifurcation diagrams and phase-plane portraits for the first cylinder in the system, for flow velocities above the critical for which a Hopf bifurcation occurs ($u_{fl} = 4{\cdot}467$). For $u = 5$, there exists a period-one motion that develops after the Hopf bifurcation (not shown); its fundamental frequency is $f_1 = 0{\cdot}83$, and it has odd harmonics (as ascertained from power spectra). For $6{\cdot}95 < u < 8{\cdot}22$, approximately, another period-1 motion develops around a pair of symmetric points, as shown in Figure 16(a) for $u = 7{\cdot}25$, with a fundamental frequency of $f_2 = 0{\cdot}64$. For $u = 8{\cdot}40$ and $u = 8{\cdot}60$, as shown in Figure 16(b, c) and in acordance with the bifurcation diagram, a local period-2 motion (of frequency $f_3 = f_2/2$), followed by a period-3 motion ($f_4 = f_2/3$), may be observed around the two symmetric points already mentioned. In Figure 16(d), for $u = 9{\cdot}075$, the motion of the system is chaotic around these two symmetric points, while in Figure 16(e), for $u = 9{\cdot}085$, the system is chaotic around only one of them, depending on the initial conditions chosen.

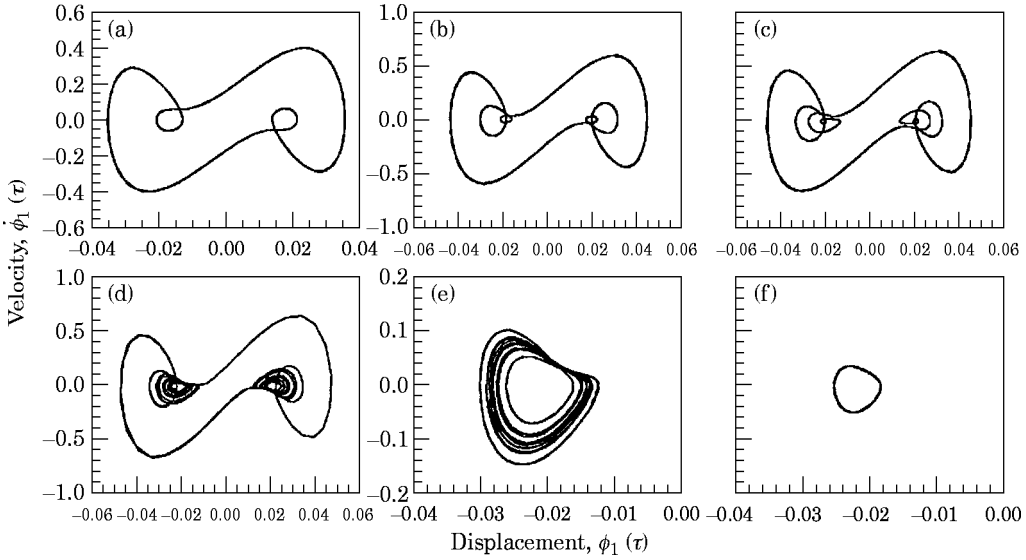

Figure 16. Phase-plane plots of $\dot{\phi}_1(\tau)$ versus $\phi_1(\tau)$ at (a) $u = 7{\cdot}25$, (b) $u = 8{\cdot}40$, (c) $u = 8{\cdot}60$, (d) $u = 9{\cdot}075$, (e) $u = 9{\cdot}085$ and (f) $u = 9{\cdot}25$, obtained with the second model, for Case 2: $h = 0{\cdot}5$ and $f = 0$.

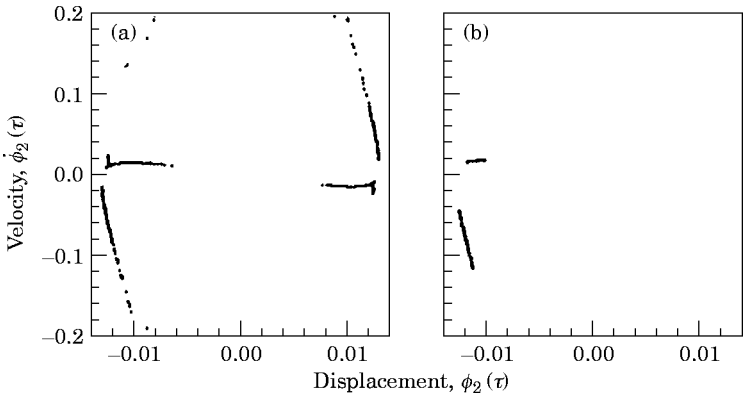

Figure 17. Poincaré sections of $\dot{\phi}_2(\tau)$ versus $\phi_2(\tau)$ when $\dot{\phi}_1(\tau) = 0$ for (a) $u = 9{\cdot}075$ and (b) $u = 9{\cdot}085$, obtained with the second model, for Case 2: $h = 0{\cdot}5$ and $f = 0$.

For higher flow velocities, a reverse period-doubling cascade takes place, for which a period-4 motion may be observed for $u = 9{\cdot}09$ (not shown here, but for which $f_1 = 0{\cdot}39$); a period-2 motion for $u = 9{\cdot}10$ ($f_2 = 0{\cdot}78$), which is followed by period-1, as seen in Figure 16(f) for $u = 9{\cdot}25$ ($f_3 = 1{\cdot}56$). The motion eventually reduces to a fixed point for $u > 9{\cdot}30$.

For (a) $u = 9{\cdot}075$ and (b) $u = 9{\cdot}085$, some Poincaré sections were constructed and they are shown in Figure 17(a, b); although uninteresting in shape, they are characteristic of chaotic motion.

Therefore, this case, according to *Model 2* also, has a very rich dynamical behaviour. In summary, chaos arises through period n motions with n = 1–4; then a reverse period-doubling sequence takes place, back to period-1 motion; the motion finally reduces to a fixed point.

5.3. DISCUSSION

In Section 5, the dynamical behaviour of this system (Case 2) has been analyzed according to both *Model 1* and *Model 2*. From a qualitative point of view the behaviour of the system for the two models is the same. By comparing the bifurcation diagrams, phase plane portraits, power spectra and Poincaré sections for this case, obtained with the non-linear Model 1 (Figure 10) and with the linearized Model 2 (Figure 15), it may be concluded that both models predict that chaotic motion occurs through period n motions, followed by a reverse period-doubling sequence, and the motion ultimately reduces to fixed points.

Differences in the quantitative sense do exist, as expected, and they may be seen in Table 2. In this table, the critical flow velocities u_{fl}, u_{1b}, u_{2b}, u_{ch} correspond to u for flutter, period-1 motion around two symmetric points, period-2 motion around these two points, and chaos; the maximum displacements for the first cylinder, $\phi_{1\max}$, and the fundamental

TABLE 2

Case 2 for Model 1 and Model 2

	u_{fl}	u_{1b}	u_{2b}	u_{ch}	$\phi_{1\max}$ ($u = u_{fl}$)	$\phi_{1\max}$ ($u = u_{1b}$)	f_1 ($u = u_{fl}$)	f_1 ($u = u_{1b}$)
Model 1	4·65	6·95	8·09	8·23	0·0037	0·0298	1·02	0·59
Model 2	4·50	6·89	8·24	8·98	0·0034	0·0320	0·83	0·64

TABLE 3

Routes to chaos for Model 1 *and Model* 2

	$h = 0{\cdot}2$		$h = 0{\cdot}5$	
f	Model 1	Model 2	Model 1	Model 2
0	← Periodic motions above 2 symmetrical points; chaos, → Period-bubbling motions; *period* 1; fixed points			
0·2	Periodic Fixed points No chaos	Periodic No chaos	*Period* 2, 4, 8 Chaos Fixed points	*Period* 2,4, 8 Chaos
0·4	← *Period* 2, 4, 8 motions; chaos →			
	Fixed points		Fixed points	
0·6	*Period* 2, 4, 8 Chaos Fixed points	*Period* 2, 4, 8 Chaos	*Period* 1 Quasiperiodic Chaos Fixed points	*Period* 2, 4, 8 Chaos
0·8	*Period* 2, 4, 8 Chaos Fixed points	*Period* 1, 2, 1 Quasiperiodic No chaos	Periodic Fixed points No chaos	*Period* 2, 4, 8 Chaos

frequencies f_1, are calculated for u_l and u_{1b}. The percentage difference in these key parameters has been calculated; *diff* (defined in Section 4.3) has values between 0·9 and 9% for u, between 7·4 and 8·0% for $\phi_{1\max}$, and between 8·5 and 18·6% for f_1.

6. CONCLUSIONS

The main purpose of this paper was to study the dynamics of the articulated system in annular flow by means of two versions of an analytical model: one (*Model 2*), in which the equations of motion (apart from "impact"-type forces) are linearized, and the other (*Model 1*) where the geometrical non-linearities are taken into account by retaining third-order terms in the Taylor expansions of the pertinent terms. The question was: how close, if at all, are the results in the two cases? The importance of this question is appreciated upon realizing that a considerable amount of work has already been done with the linearized model and some very interesting results have been obtained [10, 11]. Thus, the obvious question is this: how robust are these findings? Do they crumble if small non-linearities are introduced? (Here it should be recalled that *large* amplitude motions are not under consideration since they are precluded by the presence of the containing pipe and the narrowness of the annular gap.)

The comparison between the two models was carried out for two systems, labelled Case 1 and Case 2, both involving two articulations, and differing by the values of two parameters: h and f; h gives a measure of the tightness of the annulus and f of the degree of streamlining of the free end. For Case 1: $h = 0{\cdot}2$, $f = 0{\cdot}4$; for Case 2: $h = 0{\cdot}5$, $f = 0$.

For both cases the dynamics as predicted by the two models were found to qualitatively be substantially the same. Case 1 displayed a period-doubling route to chaos, followed by return to periodicity; back to chaos and return to periodicity a second time by the same route; and finally back to chaos a third time in the same way; terminating with collapse of the system onto fixed points at sufficiently high flow velocity according to Model 1, but not Model 2. Case 2 displayed a rather unusual dynamical behaviour. The dynamical

evolution appeared to be centred about two symmetric points in space, initially locally. Thus, period-1 local motion was succeeded by period-2, then period-3 motion, and finally chaos still in a local sense. Eventually the dynamics of the system at each of these two points became detached from any obvious connection to the other, as a reverse periodic sequence led to period-1, and then to fixed points.

The results were quite similar, quantitatively as well, as discussed in Sections 4.3 and 5.3, in terms of the values of u for some key bifurcations, frequencies and amplitudes of motion. In the case of the threshold values of u, these differences did not exceed 9%, and were usually closer; the maximum difference in the principal frequency of motions was 20%. The amplitudes were considerably closer.

Although only two cases have been presented and discussed in detail, several more were considered and the results are summarized in Table 3. Five different values of f and two values of h were examined, according to both *Model 1* and *2*. It may be seen that in some cases, especially for $f = 0{\cdot}6$ and $0{\cdot}8$, there are considerable differences in the results (comparing *Model 1* and *Model 2*); e.g., for $f = 0{\cdot}8$, $h = 0{\cdot}2$, chaos is predicted by *Model 1*, but not by *Model 2*. Another general comment is that, in many more instances, the final state predicted by the more fully non-linear model (*Model 1*) is collapse to a fixed point, which is not the case for *Model 2*; this is because the fixed point corresponds to a kind of divergence (physically, to sticking to the outer pipe wall), which involves larger amplitudes. Such sticking has often been observed in preliminary experiments with this system. Of course, *Model 2* is expected to be more realistic, because it retains third-order terms—at least, therefore, it approximates physical reality a little closer.

Broadly, it may be concluded that the results of Cases 1 and 2 of this paper (see Tables 1 and 2 and the corresponding bifurcation and phase-plane diagrams) are quite similar, both qualitatively and quantitatively. Considering the totality of the results (i.e., including Table 3) however, it is seen that agreement deteriorates with increasing f, sometimes disappearing altogether. Hence, the generality of results for $f \geqslant 0{\cdot}6$ as obtained with the "linearized" Model 2 is questionable. Fortunately, however, all the key results presented in reference [11] were obtained for systems with $f \leqslant 0{\cdot}4$.

ACKNOWLEDGMENTS

The authors gratefully acknowledge the support by NSERC of Canada and FCAR of Québec which has made this research possible.

REFERENCES

1. M. P. Païdoussis 1976 *Annals of Nuclear Energy* **3**, 19–30. Dynamics of fuel strings in axial flow.
2. N. Hamy 1971 Trebron Holdings Ltd, Montréal, Canada. The Trebron Sea Chain System.
3. M. P. Païdoussis 1986 *Proceedings of the Fifth International Offshore Mechanics and Arctic Engineering Symposium* **1**, 483–490. Stability of a chain of cylinders travelling underwater.
4. W. R. Hawthorne 1961 *Proceedings of the Institution of Mechanical Engineers* (*London*) **175**, 52–83. The early development of the Dracone flexible barge.
5. The Dunlop Rubber Company Ltd 1969 *Dunlop Dracones*, Fawley, Hants, U.K.
6. K. Hennig, E. Platen and G. Grunwald 1980 *Practical Experiences with Flow-Induced Vibrations* (E. Naudascher and D. Rockwell, eds), Berlin: Springer-Verlag, 140–143. Treatment of flow-induced pendulum oscillations.
7. F. Peterka 1991 *Journal of Fluids and Structures* **5**, 627–650. Flow-induced-impact oscillation of a spherical pendulum.
8. J. Guckenheimer and P. J. Holmes 1983 *Non-linear Oscillations*, *Dynamical Systems and Bifurcations of Vector Fields*. New York: Springer-Verlag.
9. F. C. Moon 1987 *Chaotic Vibrations: An Introduction for Applied Scientists and Engineers*. New York: John Wiley and Sons.

10. M. P. Païdoussis and R. M. Botez 1993 *Journal of Fluids and Structures* **7**, 719–750. Chaotic dynamics of articulated cylinders in confined axial flow.
11. M. P. Païdoussis and R. M. Botez 1995 *Nonlinear Dynamics* **7**, 429–450. Different routes to chaos for a three degree of freedom articulated cylinder system impacting with the outer pipe and subjected to an external axial flow.
12. M. P. Païdoussis 1966a, b *Journal of Fluid Mechanics* **26**, 717–736 and 737–751. Dynamics of flexible slender cylinders in axial flow. Part 1: theory. Part 2: experiments.
13. M. P. Païdoussis 1973 *Journal of Sound and Vibration* **29**, 365–385. Dynamics of cylindrical structures subjected to axial flow.
14. M. P. Païdoussis 1979 *Journal of Sound and Vibration* **65**, 391–417. The dynamics of clusters of flexible cylinders in axial flow: theory and experiments.
15. M. M. Munk 1924 NACA Report, No. 184, 453–468. The aerodynamic forces on airship hulls.
16. T. B. Benjamin 1961 *Proceedings Royal Society* (*London*) **261**, 457–499. Dynamics of a system of articulated pipes conveying fluid.
17. R. M. Botez 1994 Ph.D. Thesis, Department of Mechanical Engineering, McGill University, Montreal. Nonlinear dynamics of an articulated cylinder system subjected to confined axial flow.
18. G. I. Taylor 1952 *Proceedings of the Royal Society* (*London*) **214(A)**, 158–183. Analysis of the swimming of lone and narrow animals.
19. S. F. Hoerner 1958 *Fluid-Dynamic Drag; Practical Information in Aerodynamic Drag and Hydrodynamic Resistance*. Midland Park, N.J.: published by author.
20. G. S. Triantafyllou and C. Chryssostomidis 1989 *ASME Journal of Offshore Mechanics and Arctic Engineering* **111**, 208–213. The dynamics of towed arrays.
21. S. S. Chen, M. W. Wambsganss, J. A. Jendrzejczyk 1976 *Journal of Applied Mechanics* **43**, 325–329. Added mass and damping of a vibrating rod in confined viscous fluids.
22. M. P. Païdoussis and B. K. Yu 1976 *AIAA Journal of Hydronautics* **10**, 127–134. Elastohydrodynamics and stability of towed slender bodies of revolution.

APPENDIX A: ESTIMATION OF FORM FACTOR

Consider a specific case, in which the diameter of the cylinders is $D = 1{\cdot}55$ cm; hence, y_{max} is equal to $r = 1{\cdot}55/2 = 0{\cdot}775$ cm. It is recalled that the form factor $f = 0$ corresponds

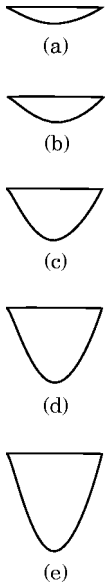

Figure A.1. Some possible shapes of the downstream end of the articulated system for form factors (a) $f \approx 0$, (b) $f \approx 0{\cdot}2$, (c) $f \approx 0{\cdot}4$, (d) $f \approx 0{\cdot}6$, and (e) $f \approx 0{\cdot}8$.

TABLE A.1

Parameters for the shapes of the downstream end shown in Figure A.1 and the corresponding estimated values of f, for paraboloidal forms of radius y, where $y^2(x) = 4a(w - x)$*—see Section 2.3*

Shape shown in Figure A.1	Value of w	a	Parameter f
(a)	0·19	0·78	0·0
(b)	0·39	0·39	0·2
(c)	0·78	0·19	0·4
(d)	1·16	0·13	0·6
(e)	1·55	0·10	0·8

to a blunt end and $f = 1$ to a streamlined end. Intermediate values of f are estimated empirically [13], as shown in Figure A.1 corresponding to the parameters of Table A.1. Dimensional quantities (w and a) are in cm. The reader is also referred to reference [22] for a more refined but much more complex treatment.